

Titre: The apparent structural hydrophobicity of cellulose nanocrystals
Title:

Auteurs: Charles Bruel, Quentin Beuguel, Jason Robert Tavares, Pierre Carreau, & Marie-Claude Heuzey
Authors:

Date: 2018

Type: Article de revue / Article

Référence: Bruel, C., Beuguel, Q., Tavares, J. R., Carreau, P., & Heuzey, M.-C. (2018). The apparent structural hydrophobicity of cellulose nanocrystals. J-FOR The Journal of Science and Technology for Forest Products and Processes, 7 (4), 13-23.
Citation: http://www.paptac.ca/fr/component/docman/doc_download/2762-subsapparent-structural-hydrophobicity-of-cellulose-nanocrystals

Document en libre accès dans PolyPublie

Open Access document in PolyPublie

URL de PolyPublie: <https://publications.polymtl.ca/4126/>
PolyPublie URL:

Version: Version finale avant publication / Accepted version
Révisé par les pairs / Refereed

Conditions d'utilisation: Tous droits réservés / All rights reserved
Terms of Use:

Document publié chez l'éditeur officiel

Document issued by the official publisher

Titre de la revue: J-FOR The Journal of Science and Technology for Forest Products and Processes (vol. 7, no. 4)
Journal Title:

Maison d'édition: PAPTAC (Pulp & Paper Technical Association of Canada)
Publisher:

URL officiel: http://www.paptac.ca/fr/component/docman/doc_download/2762-subsapparent-structural-hydrophobicity-of-cellulose-nanocrystals
Official URL:

Mention légale: ©2018. This is the author's version of an article that appeared in J-FOR The Journal of Science and Technology for Forest Products and Processes (vol. 7, no. 4) . The final published version is available at
Legal notice: http://www.paptac.ca/fr/component/docman/doc_download/2762-subsapparent-structural-hydrophobicity-of-cellulose-nanocrystals

THE APPARENT STRUCTURAL HYDROPHOBICITY OF CELLULOSE NANOCRYSTALS

Authors : Charles Bruel, Quentin Beuguel, Jason R. Tavares, Pierre J. Carreau, Marie-Claude Heuzey.
Research Center for High Performance Polymer and Composite Systems (CREPEC), Chemical Engineering Department, Polytechnique Montreal, PO Box 6079, Stn Centre-Ville, Montreal, QC H3C 3A7, Canada.

Abstract: The Teas graph of wood-based sulfuric acid-hydrolyzed cellulose nanocrystals (CNCs) was plotted based on sedimentation tests in a set of 25 common solvents. Comparisons with those of sucrose and dextran, taken as equivalents for cellobiose (cellulose repeating unit) and amorphous cellulose, respectively, highlighted the amphiphilic nature of CNCs. In the absence of any chemical arguments, the hydrophobic behavior displayed is thought to be caused by the exposition of (200) lattice planes at the CNC surface. This apparent structural hydrophobicity may be exploited to achieve the dispersion of CNCs in some mildly-non polar matrices such as poly(ethylene glycol) and poly(lactic acid). The Teas graph is a useful tool to predict the dispersibility potential of CNCs and to select a proper solvent for nanocomposite preparation

Keywords: Biomaterials; Nanocomposites; Cellulose nanocrystals; Hansen solubility parameters; Teas graph.

INTRODUCTION

Cellulose is one of the most abundant biopolymers on earth as it may be found in land plants, algae, bacteria, fungi, and sea animals such as tunicates [1, 2]. Wood, however accounts for 93 % of the industrial needs in cellulosic fibers [3]. Cellulose coexists in the latter with hemicellulose, lignin and extractives [1, 4]. The largest cellulose-only elements in plants are called elementary microfibrils [5]. Although the debate is not settled yet, biological observations suggest that, in wood and in most land-plants, they are made of ~ 36 cellulose chains, corresponding to a cross section of roughly 10 to 15 nm² [6, 7, 8]. Any material resulting from the aggregation of a few adjacent elementary fibers is called a cellulose nanofiber (CNF). These CNFs are arranged in successions of crystalline and amorphous sections of cellulose chains, where crystalline parts account for the rigidity of the elementary fibers, while amorphous ones account for their normal flexibility [1]. Cellulose nanocrystals (CNCs) are the particles obtained by the extraction of the crystalline regions of the CNFs, usually through an acid hydrolysis [1, 9]. CNCs and CNFs are both labelled as nanocellulose.

Long restricted to laboratory uses [10], nanocellulose is now producible at industrial scale and represents a new outlet for the pulp and paper industry. Canada is at the forefront with industrial units for the production of CNFs by Kruger Biomaterials (www.biomaterials.kruger.com) in Trois-Rivières (Québec, Canada, maximum production capacity of 5 tons per day) and of CNCs by Celluforce (www.celluforce.com) in Windsor (Québec, Canada, maximum production capacity of 1 ton per day) [9, 11]. Its main markets in 2017, in term of value, are those of composites (30 %), of paints, films, and coatings (15 %), and of pulp and papers (14 %) [10]. Composites indeed represent a natural application for nanocellulose and especially for CNCs, which have a theoretical Young's modulus of 208 GPa in the cellulose chain direction [12] thanks to their high crystallinity [13]. Its Young's modulus is close to that of steel [2]. Experimentally a value of 105 GPa was obtained through Raman spectroscopy [14]. These high mechanical properties, coupled with their light density (~ 1.605 g·cm⁻³) [2, 7, 15, 16], make CNCs an interesting biosourced nanofiller for reinforcement of polymers [1, 17, 18].

Focusing on wood-based CNCs, the main issue lies with their low affinity for conventional non-polar matrices such as poly(propylene) (PP) [19]. Good dispersion results have, however, been reported in the case of some mildly non-polar systems such as poly(ethylene glycol) (PEG) [20, 21, 22, 23] or poly(lactic acid) (PLA) [24, 25,

26], as well as for polar matrices such as poly(vinyl alcohol) (PVOH) [27]. An efficient tool is lacking to compare these dispersion results and assess the dispersibility potential of CNCs in polymer matrices.

Hildebrand proposed a thermodynamic approach to quantify the affinity -the cohesion- of molecules with their environment [28]. The Hildebrand solubility or cohesion parameter, δ_T (MPa^{1/2}), is defined as the square root of the cohesive energy density, CED (MPa), itself the ratio of the total cohesive energy of the system, E_T (J), normalized by the molar volume of the compound, V_m (m³·mol⁻¹), to avoid size effects (Eq. 1) [29]. Building on Hildebrand's work [28], Hansen proposed in the sixties a way to split the cohesive energy into its three main components E_D , E_P , and E_H (J), resulting respectively from the dispersion forces, the dipole-dipole and the hydrogen bonding interactions [29, 30, 31]. The corresponding Hansen solubility parameters (HSP) are labelled δ_D , δ_P , and δ_H (MPa^{1/2}). They are linked to Hildebrand's parameter via Eq. 2. Initially developed to characterize the solubility of dyes and pigments in the paint industry, HSP have proven to be relevant to other industries since then [29]. Teas proposed to represent HSP as their percent fractions in a triangular graph to ease their visualization (Eqs. 3 to 5) [33].

$$\delta_T = \sqrt{CED} = \sqrt{\frac{E_T}{V_m}} \quad (1)$$

$$\delta_T^2 = \delta_D^2 + \delta_P^2 + \delta_H^2 \quad (2)$$

$$f_D = 100 \frac{\delta_D}{\delta_D + \delta_P + \delta_H} \quad (3)$$

$$f_P = 100 \frac{\delta_P}{\delta_D + \delta_P + \delta_H} \quad (4)$$

$$f_H = 100 \frac{\delta_H}{\delta_D + \delta_P + \delta_H} \quad (5)$$

This approach may prove to be pertinent in the field of nanocellulose composites. Recently, the group of Youngblood [34, 35] published Teas graphs for the characterization of CNCs and functionalized CNCs based on sedimentation tests in various solvents. Although these pioneering works establish the potential of HSP as a tool to determine the affinity of CNCs for exogenous media, the low number of solvents tested (5 to 9) [34, 35] as well as the methodology employed do not allow for any conclusions. Indeed, while sedimentation is an effective test to characterize the HSP of fillers and particles, absolute sedimentation times, t_{sed} (h), have to be corrected by the difference in densities between the solid, ρ_p (g·cm⁻³), and the solvent, ρ_s (g·cm⁻³), and by the solvent viscosity, η_s (mPa·s) [29]. This correction insures that what is measured is the affinity of the solid for the surrounding media and not the differences in densities or in viscosities within the set of solvents. Sedimentation tests must thus be compared for a same relative sedimentation time, RST (s²·m⁻²). Corresponding absolute sedimentation times, t_{sed} (s), may be calculated according to Eq. 6 [29].

$$t_{sed} = RST \frac{\eta_s}{\rho_p - \rho_s} \quad (6)$$

Here, we report the Teas graph of wood-based sulfuric acid-hydrolyzed CNCs in a large set of 25 solvents. We compare our results with those published in the literature [31] for sucrose and dextran (Fig. 1). They are respectively considered as equivalent to cellobiose, the repeating unit of cellulose, and to amorphous cellulose [29]. We aim at understanding the influence of the chain crystalline molecular assembly over their dispersibility potential. Finally, through the example of a water based CNCs/PEG solvent casting, we provide a demonstration of how Teas graphs may be used to elaborate protocols for the dispersion of CNCs in polymer matrices.

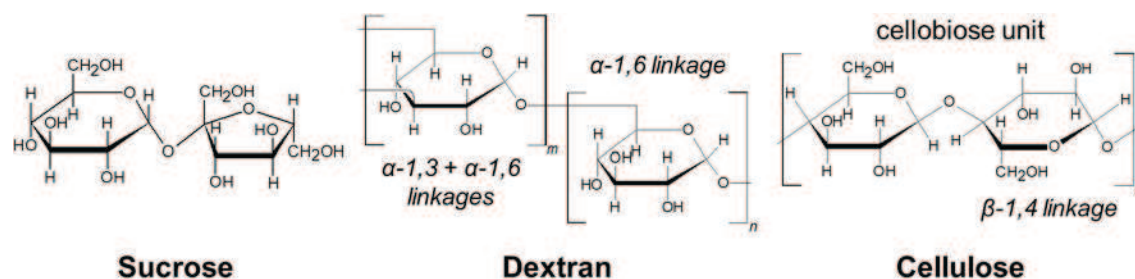


Fig. 1 – Chemical formulae of sucrose, dextran, and cellulose. Dextran is a branched polymer of anhydroglucose units linked either in α -1,6, or both in α -1,6 and α -1,3. It is an equivalent of amorphous cellulose [29, 31]. Cellulose is a polymer of cellobiose, itself a dimer of β -1,4-anhydroglucose rings [1]. Sucrose is used as an equivalent of cellobiose.

MATERIALS

Cellulose nanocrystals, produced from the sulfuric acid hydrolysis of Kraft wood pulp, followed by neutralization with sodium hydroxide (NaOH), were provided by Celluforce (Montréal, QC, Canada), as a spray-dried powder. X-Ray energy dispersive spectroscopy (EDX) measurements through a Tabletop Hitachi TM3030+ scanning electron microscope (SEM) operating at 15 kV determined that there are 3.4 sulfate half ester groups ($\text{O-SO}_3\text{H}$) per 100 anhydroglucose units [36]. The average length $L_0 \sim 165$ nm and width $l_0 \sim 13$ nm of CNC nanoparticles were obtained based on the measurements of at least 100 individual particles diluted at 0.001 wt% in water, using transmission electronic microscopy (TEM) with a bright field imaging Jeol JEM 2100F, operating at 200 kV [36]. The density of CNC was assumed to be $1.605 \text{ g}\cdot\text{cm}^{-3}$. Particles were employed as received without any pre-treatment. In his original work, Hansen used dextran C (British Drug Houses) and commercially available sucrose [31]. Purified Milli-Q water at a resistivity of $18.2 \text{ M}\Omega\cdot\text{cm}$ was used. Solvents were purchased at high purity grades from commercial suppliers. Their densities and viscosities were taken from the literature and are reported in the appendices. Poly(ethylene glycol) (PEG) was purchased from Sigma Aldrich (Oakville, ON, Canada), characterized, from the technical data sheet, by a density of $1.14 \text{ g}\cdot\text{cm}^{-3}$ and a number average molar weight of $20,000 \text{ g}\cdot\text{mol}^{-1}$.

PROTOCOLS

Sedimentation tests

0.1 g of CNCs were dispersed in 10 mL of the different solvents in a glass container with a radius of 2.1 cm, placed in an ice bath to avoid overheating, through an ultrasonic treatment at a frequency of 20 kHz, a power of $\sim 25 \text{ W}$ applied with a pulse cycle of 5 s ON and 2 s OFF for a total energy of $10,000 \text{ J}\cdot\text{g}_{\text{CNCs}}^{-1}$. The resulting CNC suspensions ($10 \text{ mg}\cdot\text{mL}^{-1}$) were allowed to rest at 25°C for a relative sedimentation time $RST = 5.9 \times 10^{10} \text{ s}^2\cdot\text{m}^{-2}$. This corresponds for instance to an absolute sedimentation time, t_{sed} , of 6.0 h in acetone, 24 h in water, or 568 h in ethylene glycol (Table 1).

Nanocomposites preparation

2 g of CNCs were dispersed in 38 mL of Milli-Q water, leading to a concentration of $5.2 \text{ mg}\cdot\text{mL}^{-1}$, in a glass container with a radius of 2.1 cm placed in an ice bath to avoid overheating, using an ultrasonic treatment at a frequency of 20 kHz, a power of 50 W applied with a pulse cycle of 1 s ON and 1 s OFF for a total energy of $10,000 \text{ J}\cdot\text{g}_{\text{CNCs}}^{-1}$. The CNC/water suspension was mixed in a PEG/water solution so that the final weight concentration of CNCs and PEG were 0.1 and 40 wt%, respectively. The suspension was then diluted one

hundred times with water in order to obtain a thin film after drying a droplet for 30 min at room temperature. Evaporation of the water yields a nanocomposite of PEG filled with 0.25 wt% of CNCs. The nanocomposite was observed using a bright field imaging Jeol JEM 2100F TEM, operating at 200 kV. Beuguel et al. performed the rheological characterization of these CNCs/PEG nanocomposites [23].

RESULTS AND DISCUSSION

Sedimentations tests

Pictures of the different vials (see appendices) were taken on 3 different backgrounds and a qualitative grade was attributed to the different dispersion states. Four different behaviors were observed for CNCs, from best (3) to worst (0) dispersibility (Fig. 2, Table 1):

- 3-Good dispersion: no sediment at the bottom of the vial and the suspension is transparent.
- 2-Partial dispersion: a sediment is present at the bottom of the vial and the suspension is opaque.
- 1-Weak dispersion: a sediment is present at the bottom of the vial and the suspension is slightly turbid.
- 0-No dispersion: a sediment is present at the bottom of the vial and the suspension is transparent.



Fig. 2 – Dispersibility scale for sedimentation tests. From left to right, and from the best to the worst, 4 levels of dispersion were observed: 3-good, 2-partial, 1-weak, and 0-none. Pictures were taken on different backgrounds (from top to bottom) to help with the evaluation. Solvents presented here are from left to right: dimethylsulfoxide, N,N-dimethylformamide, 1-propanol, and 1,4-dioxane.

Data for sucrose and dextran were extracted from the literature [31]. It should be noted that in his original work, Hansen distinguished between 6 different levels of dispersibility [31]. On his scale, 1 was the best, followed by 2, 3, 4, 5, and 0 in this order. 0 corresponded to the worst dispersibility. Comparing different qualitative scales is always tedious. Fortunately, while some of the materials tested by Hansen exhibited intermediate behaviors (grades 2 to 5), it was not the case for sucrose and dextran, for which dispersion was either found to be optimal (grade 1) or minimal (grade 0) [31]. The only assumption needed to compare the results is thus that best (this work's grade 3) means best (Hansen's grade 1) and that worst (this work's grade 0) means worst (Hansen's grade 0).

Teas graphs

As expected for these hydroxyl-rich molecules, good solvents for sucrose and dextran are concentrated in the polar region of the Teas graph (low dispersion parameter $-f_D$ - area, which translates into high polar and hydrogen components $-f_P+f_H$ -, Fig. 3.a&b). Dispersion results are very similar for dextran when compared to sucrose, with only one poorer solvent, the dimethylformamide [31]. This results into slightly higher HSP for dextran, which is consistent for the comparison of a polymer to its monomer [29], even though sucrose is not the monomer of dextran, nor of cellulose, just another sugar of similar size. Results for CNCs, however, provide a totally different graph (Fig. 3.c). The best dispersibilities (grade = 3) were here again observed for polar solvents. However, while Hansen found no difference for dextran and sucrose dispersibility among non-polar solvents despite a fine 6 levels scale [31], we observed a sharp gradient in sedimentation states. Dispersion was clearly improved for some mildly non-polar solvents (grade = 2: chloroform, methylene dichloride) while another level of weak dispersibility (grade = 1) was observed for some intermediate solvents such as mono-alkanols, ketones, ethyl acetate and tetrahydrofuran (THF). Poor solvents (grade = 0) are the less polar ones with f_P and/or f_H below 10 % (heptane, cyclohexane, toluene, 1,4-dioxane, propylene carbonate...). Ethylene glycol and benzyl alcohols, two solvents with relatively low f_P (< 20 %) and high f_H (> 35 %), also received a 0 grade. Generally speaking, best solvents (grades 2 and 3) are those for which $f_D < 70\%$, $f_P > 10\%$ and $20\% < f_H < 40\%$. Three areas of dispersibility may be plotted from data of Fig. 3.c. They are obtained by straight-linking together the points made by the solvents of same or higher grades in the Teas graph. They correspond respectively to grades 3 (in green), 3+2 (in green+blue), and 3+2+1 (in green+blue+pink) as shown in Fig. 3.d. They highlight a peak of dispersibility toward non-polar solvents. Poor solvents are also represented in Fig. 3.d to emphasize the fact that the regions of the graph for which $f_D < 30\%$, $f_P > 45\%$ or $f_H < 10\%$ have not been probed. Indeed, there are only very few common solvents corresponding to these criteria [29, 32]. The areas plotted are thus minimum dispersibility areas and may be extendable to these non-tested regions.

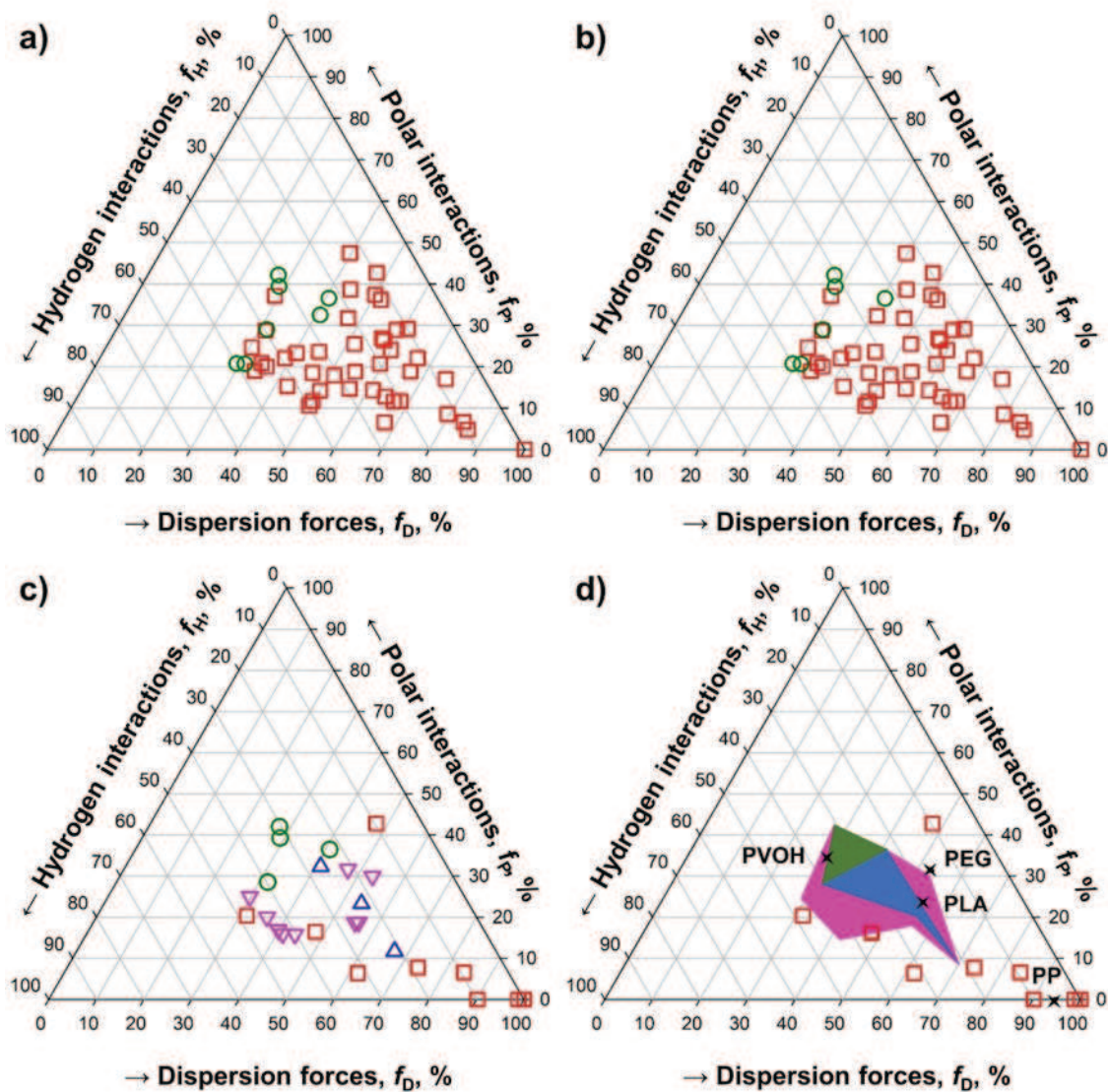


Fig. 3 – Teas graphs of sucrose (a), dextran (b), and wood-based sulfuric acid-hydrolyzed CNCs (c). f_D , f_P , and f_H , stand respectively for the fraction percents of the dispersion forces parameter, δ_D , the dipole-dipole (or polar) interactions parameter, δ_P , and the hydrogen bonding interactions parameter, δ_H (Eqs. 3 to 5). Solvents are plotted according to their grade over the dispersibility scale, from best to worst: 3 (green circles), 2 (blue triangles up), 1 (pink triangles down), 0 (red squares). (d) Minimum dispersibility areas that may be extrapolated from the Teas graph of CNCs (c). Poor solvents probed are represented on the graph to emphasize the fact that some areas of the graph remain unexplored. Some common polymers (PVOH, PEG, PLA, and PP) in which dispersibility results of wood-based sulfuric acid-hydrolyzed CNCs are available have been represented on the graph. HSPiP data are extracted from the HSPiP software database [32].

Cellulose nanocrystal apparent structural hydrophobicity

The results presented in the previous section need to be justified. Indeed, there is no chemical reason for which CNCs should be more hydrophobic than dextran, the equivalent of amorphous cellulose. The only chemical difference lies in the presence of sulfate groups at the surface of the sulfuric acid-hydrolyzed CNCs [13, 37]. However, such groups, if their influence is felt, are expected to increase, not reduce, the polarity of the

nanocrystals surface. It should be noted that an affinity of some allomorphs of crystalline cellulose for non-polar compounds has already been reported previously: be it the stable dispersion of cellulose I_β nanocrystals in chloroform [38, 39] or the specific interactions of regenerated cellulose II with hydrophobic solvents such as toluene [40] or cyclohexane [41]. If no chemical argument can explain why cellulose I_β nanocrystals are more hydrophobic than amorphous cellulose, then there has to be a structural argument. Details about the molecular assembly of cellulose chains may be found in the literature [5, 7]. Cellulose chain hydroxyl groups are all oriented in the equatorial plane of the anhydroglucose rings [42, 43]. In cellulose I_β , the OH-O hydrogen bonding network forms in this plane and cellulose units thus assemble in sheet-like structures, which stack up due to weak van der Waals interactions and CH-O hydrogen bonds (Fig. 4) [42, 44]. The resulting I_β monoclinic crystal units possess 3 main lattice planes perpendicular to cellulose chains' direction [16]: (110), ($1\bar{1}0$) and (200). The (200) plane is parallel to the sheets formed by cellulose chains while (110) and ($1\bar{1}0$) planes cut them. As a result, surfaces corresponding to the former mostly bare CH bonds while those corresponding to the latter bare hydroxyl groups, hence a difference in polarity between them.

Molecular dynamic simulations suggest that (110) and ($1\bar{1}0$) surfaces have roughly the same hydrophilicity [45, 46] and computed surface energies ($155 \text{ mN}\cdot\text{m}^{-1}$ for both) [41], while the (200) surface is much more hydrophobic [45, 47] with a lower computed surface energy ($92 \text{ mN}\cdot\text{m}^{-1}$) [41]. Molecular dynamic simulations of the wetting properties of the (110) and (200) surfaces yielded a contact angle with water of 43° and of 95° , respectively [47]. The hydrophobic behavior observed for CNCs in Fig. 3.c&d could thus be explained by the exposure of (200) lattice planes of the surface of the nanocrystals. It is expected for I_β cellulose based on crystallographic measurements [48, 49] of sulfuric acid-hydrolyzed particles and on atomic force microscopy (AFM) visualization of untreated cellulosic fibers [8]. In the latter case, the model results were also confirmed by biological observations [8, 50, 51] and the model predicts hexagonal shaped crystallites, each displaying two (110), ($1\bar{1}0$), and (200) surfaces (Fig. 4).

Such a structural hydrophobicity is a behavior that cannot be observed for amorphous cellulose (dextran, Fig. 3.b). Indeed, it is the anisotropic molecular assembly of cellulose chains in sheet-like structures that keeps all the hydroxyl groups parallel to the (200) lattice plane, where they are engaged in the hydrogen bonding network, and all the more hydrophobic CH bonds perpendicular to it. The cellulose monomer (sucrose equivalent) thus has wetting properties similar to those of amorphous cellulose (dextran equivalent), but the crystallization of the chains leads, at least for the I_β allomorph, to the display of a hydrophobic behavior caused by the molecular assembly within the nanocrystals. This is the most reasonable conclusion that can be drawn from our results based on a screening of the literature.

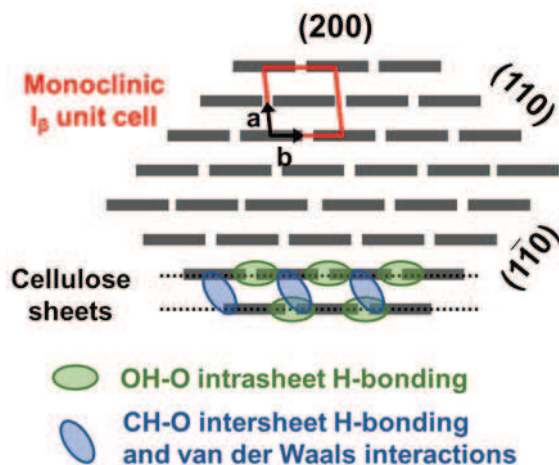


Fig. 4 – Ding and Himmel's model for cellulose chains molecular assembly [8]. Each grey rectangle represents a cellulose chain cut perpendicular to its main direction. In cellulose I_β crystalline unit cells (in red), chains assemble in sheet-like structures whose cohesion are ensured by intersheet OH-O hydrogen bonds and by weaker intrasheet CH-O bonds and van der Waals interactions. Three kind of surfaces are exposed by the crystallites: those parallel to the (110) and ($1\bar{1}0$) lattice planes cut the

cellulose sheet planes and thus expose OH groups, while the one parallel to the (200) lattice plane mostly exposes CH groups. Adapted from Li and Renneckar [44], Ding and Himmel [8], Moon et al. [7], and Nishiyama et al. [16].

Nanocomposites solvent casting

Having established that CNCs display an apparent structural hydrophobicity, which results in an affinity for some mildly non-polar solvents, it should be possible to exploit this peculiarity to favor solvent casting of nanocomposites. Indeed, polymers may also be represented in Teas graphs (Fig 3.d) [29, 32]. PVOH is at the border of the best dispersibility area (in green, grade = 3), which makes sense given that it is often presented as one of the best matrix for CNCs nanocomposites [1]. At the opposite, PP, in which CNCs dispersion is poor [19], is far outside any dispersibility area. As for the paint industry [29, 33], it thus seems that Teas graphs may represent an effective way to estimate the dispersibility potential of CNCs in various matrices. PLA, for instance, is bordering the partial dispersibility area (blue, grade = 2) and is a good medium for the dispersion of CNCs [24, 25, 26]. To produce CNCs/PLA nanocomposites, Bagheriasl et al. [25] first dispersed CNCs in DMF (solvent grade = 2), then added PLA upon stirring at 70 °C. Evaporation of the DMF yielded a nanocomposite thin film in which CNCs were dispersed individually.

PEG is just at the border of the solvent weak dispersibility region (pink, grade = 1) and it should be possible to apply a procedure similar to the one of Bagheriasl et al. [25] to disperse CNCs in PEG through solvent casting. The first step is to choose a good common solvent. To favour the dispersion of CNCs, it is preferable to pick one that belongs to the best dispersibility area such as DMSO, formamide, ethanolamine, or water. The good miscibility of PEG with water [52] makes it a natural choice for ecological issues. CNCs were thus dispersed in Milli-Q water at 5.2 mg·mL⁻¹ via an ultrasonic treatment and diluted in a PEG/Milli-Q water solution. Water evaporation resulted in a CNCs (0.25 wt%)/PEG nanocomposite thin film. Transmission electronic microscopy reveals an individual dispersion of the nanoparticles (Fig. 5), forming an apparent percolated network from a very low CNC concentration, which is consistent with previous reports by Xu et al. [21] for CNCs (1 to 10 wt%)/PEG nanocomposites obtained through water casting. Beuguel et al. performed a detailed rheological characterization of these water-casted CNCs/PEG nanocomposites [23]. They confirmed the good dispersion of the CNCs within the PEG matrix and demonstrated that a percolated network formed at volume fractions of CNCs as low as 0.15 vol% [23].

Through these examples we illustrated the potential of Teas graphs to characterize the surface chemistry of CNCs, predict their dispersibility, and choose a good solvent for a nanocomposite preparation. Previous work led by the group of Youngblood [34, 35] suggests that this method may be applicable to functionalized CNCs as well. It has to be noted that the HSP method can be applied to plot data for solvent mixtures in Teas graphs [29, 32], which opens a whole new range of possibilities for solvent casting processes.

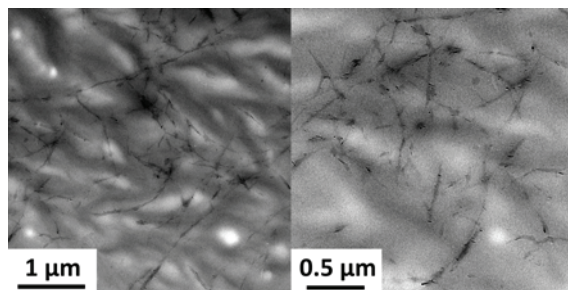


Fig. 5 – Transmission electronic imaging of a 0.25 wt% CNC/PEG nanocomposite thin film.

CONCLUSION

Cellulose nanocrystals exhibit an affinity for some mildly non-polar solvents for which dextran and sucrose, respective equivalent of amorphous cellulose and cellobiose, do not. While surface sulfatation, resulting from the sulfuric acid hydrolysis process, is expected to increase the nanocrystal polarity, its molecular assembly in sheet-like structures is believed to be responsible for this apparent hydrophobicity of CNCs. Indeed, by maintaining the hydroxyl groups of the cellulose backbone in the hydrogen bonding network of the sheets, CH hydrophobic groups are left exposed at the CNC (200) surfaces. This interpretation is backed by previous dynamic molecular modeling studies [47] and surface energy computations [41] as well as by AFM visualization [8]. Sedimentation results were represented in Teas graphs, in which dispersibility areas were plotted. It was found to be a useful tool to visualize the amphiphilic nature of CNCs and to elaborate nanocomposites solvent casting protocols as shown by an example of a water/CNC/PEG system. Literature suggests that such graphs may also be plotted in the case of functionalized CNCs. Further work will focus on the role of (200) surfaces on the apparent hydrophobicity of CNCs and on developing tools to predict and assess the dispersion of untreated CNCs and functionalized CNCs in non-polar media.

ACKNOWLEDGEMENTS

The authors are grateful to Cellulforce (Montréal, QC, Canada) for providing the cellulose nanocrystals. The financial support of FPInnovations (Pointe-Claire, QC, Canada), of PRIMA Québec, of the National Science and Engineering Research Council (NSERC) and of the Fond de Recherche du Québec – Nature et Technologies (FRQNT) is also gratefully acknowledged. Dr. W. Y. Hamad, from FPInnovations, is thanked for his personal involvement in the reviewing of this work.

REFERENCES

- [1] Hamad, W.Y., *Cellulose Nanocrystals Properties, Production and Applications*, Wiley, Chichester, UK (2017).
- [2] Habibi, Y., Lucia, L.A. and Rojas, O.J., “Cellulose Nanocrystals: Chemistry, Self-Assembly, and Applications”, *Chemical Reviews*, 110(6):3479-3500 (2010).
- [3] Smook, G.A., *Handbook for Pulp and Paper Technologists*, 1st ed., TAPPI & CPPA Publications, Atlanta, GA, USA (1982).
- [4] Fengel, D. and Wegener, G., *Wood: Chemistry, Ultrastructure, Reactions*, Walter de Gruyter, Berlin, Germany (1984).
- [5] Brown Jr, R.M., “The biosynthesis of cellulose”, *Journal of Macromolecular Science, Part A: Pure and Applied Chemistry*, 33(10):1345-1373 (1996).
- [6] Doblin, M.S., Kurek, I., Jacob-Wilk, D. and Delmer, D.P., “Cellulose Biosynthesis in Plants: from Genes to Rosettes”, *Plant and Cell Physiology*, 43(12):1407-1420 (2002).
- [7] Moon, R.J., Martini, A., Nairn, J., Simonsen, J. and Youngblood, J., “Cellulose nanomaterials review: structure, properties and nanocomposites”, *Chemical Society Reviews*, 40(7):3941-3994 (2011).
- [8] Ding, S.-Y. and Himmel, M.E., “The Maize Primary Cell Wall Microfibril: A New Model Derived from Direct Visualization”, *Journal of Agricultural and Food Chemistry*, 54(3):597-606 (2006).
- [9] Miller, J., “Nanocellulose. State of the industry. December, 2015”, *TAPPI International Conference on Nanotechnology for Renewable Materials* (2015). <http://www.tappinano.org/media/1114/cellulose-nanomaterials-production-state-of-the-industry-dec-2015.pdf>, accessed on 2017/11/05.

- [10] Dufresne, A, "La nanocellulose, le nouvel "or vert"?", *Techniques de l'Ingénieur*, Janvier-Février:46-47 (2017).
- [11] Charreau, H., Foresti, M.L. and Vázquez, A., "Nanocellulose Patents Trends: A Comprehensive Review on Patents on Cellulose Nanocrystals, Microfibrillated and Bacterial Cellulose", *Recent Patents on Nanotechnology*, 7(1):56-80 (2013).
- [12] Dri, F.L., Hector Jr, L.G., Moon, R.J. and Zavattieri, P.D., "Anisotropy of the elastic properties of crystalline cellulose I β from first principles density functional theory with Van der Waals interactions", *Cellulose*, 20(6):2703-2718 (2013).
- [13] Hamad, W.Y. and Hu, T.Q., "Structure-process-yield interrelation in nanocrystalline cellulose extraction", *Canadian Journal of Chemical Engineering*, 88(3):392-402 (2010).
- [14] Rusli, R. and Eichhorn, S.J., "Determination of the stiffness of cellulose nanowhiskers and the fiber-matrix interface in a nanocomposite using Raman spectroscopy", *Applied Physics Letters*, 93(3):033111 (2008).
- [15] Eyley, S. and Thielemans, W., "Surface modification of cellulose nanocrystals", *Nanoscale*, 6(14):7764-7779 (2014).
- [16] Nishiyama, Y., Langan, P. and Chanzy, H., "Crystal Structure and Hydrogen-Bonding System in Cellulose I β from Synchrotron X-ray and Neutron Fiber Diffraction", *Journal of the American Chemical Society*, 124(31):9074-9082 (2002).
- [17] Mariano, M., El Kissi, N. and Dufresne, A., "Cellulose Nanocrystals and Related Nanocomposites: Review of some Properties and Challenges", *Journal of Polymer Science Part B: Polymer Physics*, 52(12):791-806 (2014).
- [18] Ching, Y.C., Ali, Md.E., Abdullah, L.C., Choo, K.W., Kuan, Y.C., Julaihi, S.J., Chuah, C.H. and Liou, N.-S., "Rheological properties of cellulose nanocrystal-embedded polymer composites: a review", *Cellulose*, 23(2):1011-1030 (2016).
- [19] Bagheriasl, D., Carreau, P.J., Dubois, C. and Riedl, B., "Properties of polypropylene and polypropylene/poly(ethylene-co-vinyl alcohol) blend/CNC nanocomposites", *Composites Science and Technology*, 117:357-363 (2015).
- [20] Zhou, C., Wu, Q. and Zhang, Q., "Dynamic rheology studies of in situ polymerization process of polyacrylamide-cellulose nanocrystal composite hydrogels", *Colloid and Polymer Science*, 289(3):244-255 (2011).
- [21] Xu, X., Liu, F., Jiang, L., Zhu, J.Y., Haagensohn, D. and Wiesenborn, D.P., "Cellulose Nanocrystals vs. Cellulose Nanofibrils: A Comparative Study on Their Microstructures and Effects as Polymer Reinforcing Agents", *ACS Applied Materials & Interfaces*, 5(8):2999-3009 (2013).
- [22] Xu, X., Wang, H., Jiang, L., Wang, X., Payne, S.A., Zhu, J.Y. and Li, R., "Comparison between Cellulose Nanocrystal and Cellulose Nanofibril Reinforced Poly(ethylene oxide) Nanofibers and Their Novel Shish-Kebab-Like Crystalline Structures", *Macromolecules*, 47(10):3409-3416 (2014).
- [23] Beuguel, Q., Tavares, J.R., Carreau, P.J. and Heuzey, M.-C., "Rheological behavior of cellulose nanocrystal suspensions in polyethylene glycol", *Journal of Rheology*, 62:607-618 (2018).
- [24] Zhang, C., Salick, M.R., Cordie, T.M., Ellingham, T., Dan, Y. and Turng, L.-S., "Incorporation of poly(ethylene glycol) grafted cellulose nanocrystals in poly(lactic acid) electrospun nanocomposite fibers as potential scaffolds for bone tissue engineering", *Materials Science and Engineering: C*, 49:463-471 (2015).
- [25] Bagheriasl, D., Carreau, P.J., Riedl, B., Dubois, C. and Hamad, W.Y., "Shear rheology of polylactide (PLA)-cellulose nanocrystal (CNC) nanocomposites", *Cellulose*, 23(3):1885-1897 (2016).
- [26] Raquez, J.-M., Habibi, Y., Murariu, M. and Dubois, P., "Polylactide (PLA)-based nanocomposites". *Progress in Polymer Science*, 38(10-11):1504-1542 (2013).

- [27] Ng, T.C., Ching, Y.C., Nur, A., Ishenny, N. and Rahman, M.R., "Effect of bleaching condition on thermal properties and UV-transmittance of PVA/cellulose biocomposites", *Materials Research Innovations*, 18(sup6: ICoSEM 2013):400-404 (2014).
- [28] Hildebrand, J. and Scott, R.L., *Regular Solutions*, Prentice-Hall, Englewood Cliffs, NJ, USA. (1962).
- [29] Hansen, C.M., *Hansen Solubility Parameters A User's Handbook*, CRC Press, Boca Raton, FL, USA (2007).
- [30] Hansen, C.M., *The Three Dimensional Solubility Parameter and Solvent Diffusion Coefficient, Their Importance in Surface Coating Formulation*, PhD thesis, Technical University of Denmark, Copenhagen, Denmark (1967).
- [31] Hansen, C.M., "The universality of the solubility parameter", *Industrial and Engineering Chemistry Product Research and Development*, 8(1):2-11 (1969).
- [32] Abbott, S.J., Hansen, C.M. and Yamamoto, Y., "Hansen Solubility Parameters in Practice", software, eBook, datasets (2018). <http://www.hansen-solubility.com>, accessed on 2018/04/11.
- [33] Teas, J.P., "Graphic analysis of resin solubilities", *Journal of paint technology*, 40(516):19-25 (1968).
- [34] Peng, S.X., Chang, H., Kumar, S., Moon, R.J. and Youngblood, J.P., "A comparative guide to controlled hydrophobization of cellulose nanocrystals via surface esterification", *Cellulose*, 23(3):1825-1846 (2016).
- [35] Yoo, Y. and Youngblood, J.P., "Green One-Pot Synthesis of Surface Hydrophobized Cellulose Nanocrystals in Aqueous Medium", *ACS Sustainable Chemistry & Engineering*, 4(7):3927-3938 (2016).
- [36] Beuguel, Q., Tavares, J.R., Carreau, P.J. and Heuzey, M.-C., "Ultrasonication of spray- and freeze-dried cellulose nanocrystals in water", *Journal of Colloid and Interface Science*, 516:23-33 (2018).
- [37] Dong, X.M., Revol, J.-F. and Gray, D.G., "Effect of microcrystallite preparation conditions on the formation of colloid crystals of cellulose", *Cellulose*, 5(1):19-32 (1998).
- [38] Yu, H. and Qin, Z., "Effect of Cellulose nanocrystal on Crystallization Behavior of Poly(3-hydroxybutyrate-co-3-hydroxyvalerate)", *Advanced Materials Research*, 430-432:20-23 (2012).
- [39] Yu, H.-Y., Qin, Z.-Y., Liu, Y.-N., Chen, L., Liu, N. and Zhou, Z., "Simultaneous improvement of mechanical properties and thermal stability of bacterial polyester by cellulose nanocrystals", *Carbohydrate Polymers*, 89(3):971-978 (2012).
- [40] Sato, K., Mochizuki, H., Okajima, K. and Yamane, C., "Effects of Hydrophobic Solvents on X-Ray Diffraction Patterns of Regenerated Cellulose Membrane", *Polymer Journal*. 36(6):478-482 (2004).
- [41] Yamane, C., Aoyagi, T., Ago, M., Sato, K., Okajima, K. and Takahashi, T., "Two Different Surface Properties of Regenerated Cellulose due to Structural Anisotropy", *Polymer Journal*. 38(8):819-826 (2006).
- [42] Jarvis, M., "Cellulose stacks up", *Nature*, 426(6967):611-612 (2003).
- [43] Djahedi, C., Bergenstr hle Wohler, M., Berglund, L.A. and Wohler, J., "Role of hydrogen bonding in cellulose deformation-the leverage effect analyzed by molecular modeling", *Cellulose*, 23(4):2315-2323 (2016).
- [44] Li, Q. and Renneckar, S., "Supramolecular Structure Characterization of Molecularly Thin Cellulose I Nanoparticles", *Biomacromolecules*, 12(3):650-659 (2011).
- [45] Matthews, J.F., Skopec, C.E., Mason, P.E., Zuccato, P., Torget, R.W., Sugiyama, J., Himmel, H.E. and Brady, J.W., "Computer simulation studies of microcrystalline cellulose I β ", *Carbohydrate Research*, 341(1):138-152 (2006).
- [46] Heiner, A.P., Kuutti, L. and Teleman, O., "Comparison of the interface between water and four surfaces of native crystalline cellulose by molecular dynamics simulations", *Carbohydrate Research*, 306(1-2):205-220 (1998).

- [47] Mazeau, K. and Rivet, A., "Wetting the (110) and (100) Surfaces of I β Cellulose Studied by Molecular Dynamics", *Biomacromolecules*, 9(4):1352-1354 (2008).
- [48] Sèbe, G., Ham-Pichavant, F., Ibarboure, E., Koffi, A.L.C. and Tingaut, P., "Supramolecular Structure Characterization of Cellulose II Nanowhiskers Produced by Acid Hydrolysis of Cellulose I Substrates", *Biomacromolecules*, 13(2):570-578, 2012.
- [49] Elazzouzi-Hafraoui, S., Nishiyama, Y., Putaux, J.-L., Heux, L., Dubreuil, F. and Rochas, C., "The shape and size distribution of crystalline nanoparticles prepared by acid hydrolysis of native cellulose", *Biomacromolecules*, 9(1):57-65 (2008).
- [50] Ding, S.-Y., Liu, Y.-S., Zeng, Y., Himmel, M.E., Baker, J.O. and Bayer, E.A., "How Does Plant Cell Wall Nanoscale Architecture Correlate with Enzymatic Digestibility?", *Science*, 338(6110):1055-1060 (2012).
- [51] Ding, S.-Y., Zhao, S. and Zeng, Y., "Size, shape, and arrangement of native cellulose fibrils in maize cell walls", *Cellulose*, 21(2):863-871 (2014).
- [52] Graham, N.B., Zulfiqar, M., Nwachuku, N.E. and Rashid, A., "Interaction of poly(ethylene oxide) with solvents: 2. Water-poly(ethylene glycol)", *Polymer*, 30(3):528-533 (1988).

Table 1 – Fractional Hansen solubility parameters and sedimentation tests results for a set of 25 solvents. A qualitative grade (0 to 3) is attributed to each solvent after an absolute sedimentation time, t_{sed} , corresponding to a relative sedimentation time of $RST = 5.9 \cdot 10^{10} \text{ s}^2 \cdot \text{m}^{-2}$.

Solvents	δ^1	δ^1	δ^1	t_{sed}^2	Grade ³
	%	%	%	h	0 to 3
acetone	47.1	31.6	21.3	6.0	1
benzene	90.2	0.0	9.8	13.5	0
benzyl alcohol	47.9	16.4	35.7	155	0
2-butanol	43.9	15.8	40.3	64.5	1
chloroform	66.9	11.7	21.4	63.3	2
cyclohexane	98.8	0.0	1.2	17.5	0
dimethyl sulfoxide	40.9	36.4	22.7	63.8	3
1,4-dioxane	61.8	6.4	31.8	34.0	0
ethanol	35.9	20.0	44.1	21.8	1
ethanolamine	31.8	29.0	39.2	523	3
ethyl acetate	55.8	18.7	25.4	9.8	1
ethylene glycol	31.5	20.4	48.1	568	0
formamide	27.6	42.0	30.4	113	3
heptane	100.0	0.0	0.0	6.9	0
d-limonene	73.8	7.7	18.5	19.2	0
methanol	29.8	24.9	45.2	11.0	1
methyl ethyl ketone	53.2	29.9	16.9	7.9	1
methylene dichloride	54.1	23.2	22.6	22.6	2
N,N-dimethyl formamide	41.0	32.3	26.7	19.8	2
1-propanol	39.8	16.9	43.3	40.3	1
2-propanol	41.3	15.9	42.8	40.4	1
propylene carbonate	47.5	42.8	9.7	101	0
tetrahydrofuran	55.1	18.7	26.2	10.4	1
toluene	84.1	6.5	9.3	12.1	0
water ⁴	29.0	39.2	31.7	24 ⁵	3

¹ Data for the HSP are extracted from the HSPiP software database [32].

² Calculated thanks to the Eq. 6. Data used for solvents densities and viscosities may be found in appendices.

³ See Fig. 2.

⁴ Water has 3 sets of HSP. “1% soluble in” is the most appropriate [29, 32].

⁵ 24 h in water was chosen to establish the reference for the sedimentations tests.